Clays and Clay Minerals, Vol. 58, No. 3, 377–387, 2010.

PRECIPITATION AND TRANSFORMATION OF SECONDARY Fe OXYHYDROXIDES IN A HISTOSOL IMPACTED BY RUNOFF FROM A LEAD SMELTER

XIAODONG GAO[1,*] AND DARRELL G. SCHULZE[2]

[1] Department of Soil, Water and Environmental Science, University of Arizona, Tucson, AZ 85719-0038, USA
[2] Department of Agronomy, Purdue University, West Lafayette, IN 47907-2054, USA

Abstract—Secondary Fe(III) oxyhydroxides play a key role in controlling the mobility and bioavailability of trace metals in acidic, sulfate-rich soils, such as mining and smelter sites. Schwertmannite, jarosite, goethite, and ferrihydrite are the most common mineral phases identified in such soils. A good understanding of the precipitation and transformation of these minerals in soils is very important for predicting the mobility and long-term stability of trace metals associated with them. In the present study, bulk powder X-ray diffraction (XRD), scanning electron microscopy (SEM), synchrotron based micro-X-ray diffraction (μ-XRD), and micro X-ray fluorescence (μ-SXRF) spectroscopy were used to investigate precipitates from the surface horizon of an organic soil (Histosol) at a site that once contained a lead smelter. Soil samples were collected from 0 to ~10 cm depth during both wet and dry seasons. Goethite and akaganeite were identified as the major mineral phases in this soil. Schwertmannite and jarosite were also occasionally identified, particularly in the soil samples from dry periods. The peaks in the akaganeite XRD pattern were significantly broadened and the relative intensities of some major peaks were distinctly different compared with the diffraction pattern of synthetic akaganeite, possibly due to the effects of pH and the incorporation of sulfate. The SEM and μ-XRD data support the hypothesis that the goethite in the precipitates is not the product of direct precipitation from solution but the transformation of previously precipitated schwertmannite or akaganeite.

Key Words—Akaganeite, Fe Oxyhydroxides, Goethite, Jarosite, Precipitatation, Schwertmannite, Trace Metals, Transformation.

INTRODUCTION

Smelter operations produce large quantities of waste materials that are often rich in sulfide minerals such as pyrite (FeS_2), galena (PbS), and arsenopyrite (FeAsS), which are thermodynamically unstable under Earth-surface conditions. Abiotic and biotic weathering processes can oxidize sulfide minerals and release SO_4^{2-} and metals to the surrounding environment, forming very acidic conditions (Rohwerder *et al.*, 2003). The oxidation of pyrite by atmospheric O_2 can be expressed as:

$$FeS_{2(s)} + 7/2O_2 + H_2O \rightarrow Fe^{2+} + 2SO_4 + 2H^+ \quad (1)$$

The Fe^{2+} produced by the weathering reaction can be transported and further oxidized to Fe^{3+} and precipitated as Fe(III) oxyhydroxides (equations 2 and 3).

$$Fe^{2+} + 1/4O_2 + H^+ \rightarrow Fe^{3+} + 1/2H_2O \quad (2)$$
$$Fe^{3+} + 2H_2O \rightarrow FeOOH + 3H^+ \quad (3)$$

The Fe(III) precipitates in such acidic, sulfate-rich environments typically contain jarosite [$KFe_3(SO_4)_2(OH)_6$], schwertmannite [$Fe_8O_8(OH)_6SO_4$], goethite (α-FeOOH), and ferrihydrite ($Fe_5HO_8{\cdot}4H_2O$), depending on site-specific solution chemistry (Bigham *et al.*, 1996). Under very acidic conditions (pH < 2.5) with large sulfate concentrations, jarosite forms, whereas at slightly acidic to near-neutral pH, ferrihydrite and goethite are known to precipitate. Between pH 2.5–4.5, schwertmannite is the most common phase which precipitates (Bigham *et al.*, 1996; Yu *et al.*, 1999; Jonsson *et al.*, 2005).

Schwertmannite is a poorly crystalline mineral that forms from oxidized, sulfate- and Fe-rich solutions, and is often the primary component of the precipitates formed from sulfate-rich mine waters (Bigham *et al.*, 1990). Natural schwertmannite contains ~10–15% sulfate by weight, which converts to an Fe/S molar ratio ranging from 5 to 8 and a structural formula varying between $Fe_8O_8(OH)_{4.8}(SO_4)_{1.6}$ and $Fe_8O_8(OH)_6SO_4$ (Bigham *et al.*, 2002). Although the structure of schwertmannite has yet to be properly defined, schwertmannite is generally considered to have a tunnel structure similar to that of akaganeite (Bigham *et al.*, 1990). In akaganeite, the structure is stabilized by Cl^-, F^-, or OH^- occupying every second cavity, whereas in schwertmannite the structure is stabilized by SO_4^{2-} in the cavities, with excess SO_4^{2-} absorbing onto its surface sites (Jonsson *et al.*, 2005; Regenspurg and Peiffer, 2005). Due to size restrictions, the large SO_4^{2-} ion cannot occupy the structural cavities without sharing the O atoms with the surrounding Fe atoms (Fukushi *et al.*, 2003). Thus, the unit cell of schwertmannite is severely distorted compared to the akaganeite structure, resulting in the poor

* E-mail address of corresponding author:
xdgao@email.arizona.edu
DOI: 10.1346/CCMN.2010.0580308

crystallinity of schwertmannite. Compared to akaganeite, the XRD pattern of schwertmannite has broad, weak peaks, and the d_{110} peak at 7.39 Å of akaganeite is not present (Cornell and Schwertmann, 2003). In addition to SO_4^{2-}, chromate (CrO_4^{2-}), arsenate (AsO_4^{3-}), and molybdate (MoO_4^{2-}) can also be incorporated into the tunnels of schwertmannite (Murad *et al.*, 1994; Linehan *et al.*, 1997; Reagenspurg and Peiffer, 2005; Carroll and Richmond, 2008).

In contrast to other common Fe oxyhydroxides, akaganeite (β−FeOOH) is rare in soils but has often been observed as a corrosion product of metallic iron in chloride-containing marine environments (Cai *et al.*, 2001; Remazeilles and Refait, 2007). The crystal structure of akaganeite contains double chains of $FeO_3(OH)_3$ octahedra sharing corners to produce square tunnels extending parallel to the *c* axis, in which Cl^- ions reside (Deliyanni *et al.*, 2003; Fukushi *et al.*, 2003). Precipitation of akaganeite from pure aqueous $FeCl_3$ solutions leads to small surface area, well formed crystals, and sharp peaks in XRD patterns (Deliyanni *et al.*, 2003). The addition of other anions, such as bicarbonate (HCO_3^-) or sulfate (SO_4^{2-}), during precipitation processes have been reported, however, to partially disrupt the crystalline structure, leading to large surface areas and broad peaks in its XRD patterns (Deliyanni *et al.*, 2003).

Due to their abundance in soils and high affinity for the trace metals (*e.g.* As, Pb, and Zn), secondary Fe(III) precipitates are important sinks for trace metals in the environment and may significantly reduce the mobility and bioavailability of metals through adsorption, coprecipitation, or a combination of the two processes (Ford, 2002; Fukushi *et al.*, 2003). Poorly crystalline phases, such as ferrihydrite, schwertmannite, and akaganeite often have large active surface areas for metal adsorption. Schwertmannite and akaganeite are particularly suitable sinks for metal oxyanions, such as AsO_4^{3-} and CrO_4^{2-}, because, in addition to their large surface areas, oxyanions can easily incorporate into the square tunnel structures as mentioned above (Regenspurg and Peiffer, 2005). Akaganeite has been reported as a low-cost, effective absorbent for the removal of As(V) (Deliyanni *et al.*, 2003), Cr(VI) (Lazaridis *et al.*, 2005), and Cd^{2+} (Deliyanni and Matis, 2005) from aqueous solutions or wastewaters.

Furthermore, the Fe(III) precipitates are seldom identified as one pure mineral phase but often contain two or more phases (Jonsson *et al.*, 2006). The occurrences of mixtures are common because ferrihydrite, schwertmannite, and akaganeite are metastable and may transform into other, more thermodynamically stable phases over timescales of weeks to months (Yu *et al.*, 1999; Ford, 2002; Schroth and Parnell, 2005; Acero *et al.*, 2006; Burton *et al.*, 2006; Jonsson *et al.*, 2006). The transformation from poorly crystalline phases to more ordered crystalline phases such as goethite or hematite may reduce the surface areas of these minerals, and thereby result in desorption of adsorbed trace metals. The time scale of the transformation depends on temperature, pH, and the presence of other anions and cations (Dixit and Hering, 2003; Jonsson *et al.*, 2005). For example, schwertmannite is only stable at low pH. At pH > 4, it transforms spontaneously to goethite *via* solution and releases all its structural SO_4^{2-} and adsorbed metals (Cornell and Schwertmann, 2003):

$$Fe_8O_8(OH)_6(SO_4)_{(S)} + 2H_2O \rightarrow 8FeOOH_{(S)} + 2H^+ + SO_4^{2-} \quad (4)$$

The transformation process is slower under conditions of large sulfate concentrations, low pH, and low temperature (Bigham *et al.*, 1990, 1996; Fukushi *et al.*, 2003; Jonsson *et al.*, 2005). Large amounts of adsorbed arsenate in schwertmannite have also been shown to inhibit the transformation to goethite (Fukushi *et al.*, 2003, Regenspurg and Peiffer, 2005). Thus, the adsorption of As(V) makes the schwertmannite more stable and an effective long-term As(V) sink.

The objective of this study was to characterize the *in situ* mineralogy of Fe-rich precipitates that formed in the surface horizon of an organic soil that received runoff from the site of a former lead smelter, and to elucidate the precipitation and transformation of the secondary Fe(III) minerals and their potential impacts on the mobility and bioavailability of the adsorbed trace metals.

MATERIALS AND METHODS

Field sampling

Samples were collected from a soil on a site in Indiana that hosted a lead smelter from the 1920s to the 1980s. The soil, mapped as a Houghton muck (euic, mesic, Typic Haplosaprist), is in a wetland at the edge of the site and has apparently received runoff from the site over the years. The site has been remediated and is covered with common reed (*Phragmites australis*) and cattail (*Typha* sp.). A small area of contaminated soil that remains in one area was the sampling site for this study. The water table is at or slightly above the soil surface for much of the year, but the surface layer dries during dry periods.

Field sampling was carried out between March 2004 and August 2005. Soil samples were collected from the surface to a depth of ~10 cm during both wet and dry periods. The samples were sealed immediately in polyethylene freezer bags, frozen in liquid N_2 on site, and then transported to the laboratory and freeze-dried. The pH of the surface horizon was measured in the field during wet periods and was slightly acidic at ~5.30. A detailed description of the field sampling is given elsewhere (Gao and Schulze, 2010).

Aqueous extraction and chemical analysis for major anions

Freeze-dried soil samples were extracted in duplicate in 35 mL polyethylene centrifuge tubes at a 1:1

solid:solution ratio in nanopure water following the methods of Rhoades (2003). The suspensions were equilibrated on a mechanical shaker for 1 h, and centrifuged at 5000 rpm at 25ºC for 30 min. The supernatant was aspirated and filtered through a 0.45 μm nominal pore-size syringe filter. Anion concentrations were determined using ion chromatography (Dionex Ion Chromatograph DX-500, Sunnyvale, California, USA) with an AS-11 column and a NaOH mobile phase.

Mineral synthesis

Goethite, akaganeite, and schwertmannite were synthesized in the laboratory following the methods of Cornell and Schwertmann (2003) with minor modifications in order to compare their surface morphologies and crystal structures with their natural analogues. All chemicals were A.C.S. (American Chemical Society) certified reagents and used without further purification.

Goethite was prepared by first precipitating ferrihydrite by adding 180 mL of 5 M KOH (Mallinckrodt) to 100 mL of 1 M $Fe(NO_3)_3 \cdot 9H_2O$ (Sigma-Aldrich) solution. The suspension was diluted to 2 L with deionized water and held in a closed polypropylene flask at 70ºC for 60 h. The precipitate was then washed with deionized water and dried at 50ºC. To precipitate akaganeite, 2 L of 0.1 M $FeCl_3 \cdot 6H_2O$ (Mallinckrodt) solution was kept in a closed polypropylene flask at 70ºC for 48 h. The precipitate was washed with deionized water and air dried at room temperature. Schwertmannite was synthesized by adding 10.8 g of $FeCl_3 \cdot 6H_2O$ (~40 mM Fe^{3+}) and 3 g of Na_2SO_4 (Mallinckrodt) (~10 mM SO_4^{2-}) to 2 L of deionized water at 60ºC. The solution was maintained at 60ºC for an additional 12 min, and then was allowed to cool to room temperature before being transferred into dialysis tubing (Spectra/Por 7 1000 MWCO). The suspension was dialyzed against deionized water, which was renewed daily for ~30 days, and then freeze dried.

Bulk XRD analysis

Bulk powder XRD patterns were obtained using a PANalytical X'Pert PRO MPD X-ray diffraction system (PANalytical, Almelo, The Netherlands) equipped with a PW3050/60 θ-θ goniometer and a Co-target X-ray tube operated at 40 kV and 35 mA. Aliquots consisting of ~0.5 g of sample were ground finely (<50 μm) and homogenized in an agate mortar and pressed powder mounts were prepared in 15 mm × 20 mm Al sample holders. The samples were scanned from 2.1 to 80º2θ at 0.05º steps with 60 s of measurement time per step.

Synchrotron μ-XRD and μ-SXRF analysis

Synchrotron μ-XRD and μ-SXRF spectra were collected at the National Synchrotron Light Source (NSLS) on beamline X26A at Brookhaven National Laboratory (Brookhaven, New York, USA). Freeze-dried soil samples were examined under a binocular microscope, and aggregates ~100−200 μm in diameter were selected and mounted on Kapton tape (DuPont) supported across 50 mm × 50 mm cardboard frames. A monochromatic beam with a wavelength near 0.72 Å (actual wavelength varied slightly from run to run) was focused to a nominal size of 10 μm × 10 μm by Kirkpatrick-Baez mirrors. The 2D micro XRD data were collected in transmission mode using a Bruker SMART 1500 CCD area detector with 1024 × 1024 pixel resolution using a 120 s exposure time per sample. The detector was calibrated against corundum (α-Al_2O_3) and Ag behenate [$CH_3(CH_2)_{20}COOAg$] diffraction standards. Pattern integration was performed in FIT2D (A. Hammersley, European Synchrotron Radiation Facility, Grenoble, France) to convert the two-dimensional patterns to one-dimensional 2θ *vs*. intensity patterns. The X'Pert High Score Plus software package (PANalytical, Almelo, The Netherlands) was used for phase identification using the PDF-4+ powder diffraction database.

The μ-SXRF spectra were collected simultaneously for each aggregate using a Canberra SL30165 Si(Li) detector at energy >17.0 keV with 300 s exposure time per sample.

SEM analysis

The Kapton tape holding the aggregates examined by synchrotron μ-XRD and μ-SXRF was removed carefully from the cardboard frames and remounted on Al stubs so that the same aggregates could be examined by SEM. The samples were sputter coated with AuPd, and imaged in a JEOL JSM-840 SEM using 5 kV accelerating voltage, 22−24 mm working distance, and 3×10^{-11} mA probe current. Digital images were captured using 1280 × 960 pixel resolution and 160 s dwell time.

RESULTS AND DISCUSSION

Characterization of synthetic Fe oxyhydroxides

The synthetic minerals were characterized using bulk powder XRD and SEM. Synthetic schwertmannite yielded eight broad peaks, indicating its poor crystallinity. Both peak positions and intensities are in good agreement with the PDF pattern 00-047-1775 for schwertmannite (Figure 1). The 212 reflection at 0.255 nm is the strongest peak in the pattern. The SEM image does not show the typical pin-cushion morphology of schwertmannite (Figure 2a). Instead, the material appears to be a porous mass without distinctive morphology. Similar morphology for synthetic schwertmannite was previously reported by Webster *et al.* (1998).

The synthetic akaganeite was a pure, well defined mineral phase with sharp peaks in its diffraction pattern and matches well with the PDF pattern 00-042-1315 for akaganeite (Figure 1). The SEM image displays the typical somatoid (spindle) morphology (Figure 2b) of

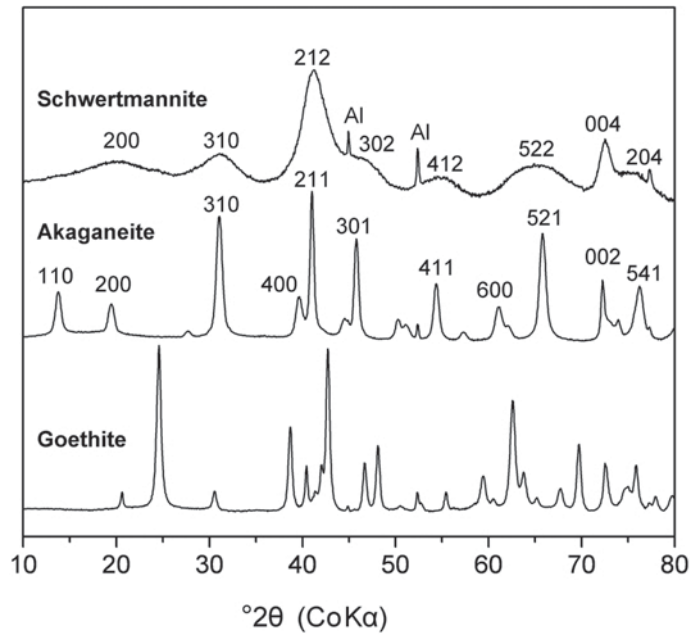

Figure 1. Bulk powder XRD patterns of the synthetic schwertmannite, akaganeite, and goethite. Al = peaks from Al sample holder. Numbers indicate Miller indices of selected peaks.

akaganeite. The somatoids are ~0.10 μm long and ~0.02 μm wide, and are highly aggregated.

The XRD pattern for the synthetic goethite indicated a pure, well defined mineral phase, matching almost perfectly PDF pattern 00-029-0713 (Figure 1). The SEM image shows the typical acicular (needle-shape) morphology, where the needle axis is parallel to the *c* axis (Figure 2c) (Bigham *et al.*, 2002). The lengths of the crystals range from several hundred nm to ~1 μm.

Mineralogy of the natural-surface precipitates

A representative bulk XRD pattern (Figure 3) of the natural precipitates sampled during a wet period consisted of a mixture of three phases, including quartz (SiO_2), goethite (α-FeOOH), and a poorly crystalline mineral phase. The bulk XRD patterns of the samples from dry periods exhibited similar features, except that they contain gypsum ($CaSO_4 \cdot 2H_2O$) which is absent from the samples from wet periods (data not shown). In addition to goethite, ferrihydrite and schwertmannite are common poorly crystalline Fe(III) oxyhydroxides frequently observed in acidic, sulfate-rich soils depending on pH, temperature, and the presence and concentration of foreign anions (*e.g.* SO_4^{2-} and Cl^-) and organic matter (Yu *et al.*, 1999; Singh *et al.*, 1999; Carlson *et al.*, 2002). However, the mineralogical complexity of the natural sample made definitive identification difficult. Further investigation was conducted using synchrotron μ-XRD.

About 80 individual μ-XRD patterns were obtained from small aggregates picked from the soil samples. The poorly crystalline phase in the bulk XRD (Figure 3) was identified successfully as akaganeite (β-FeOOH) by μ-XRD. The peak positions of the mineral are in good agreement with PDF pattern 00-042-1315 for akaganeite (Figure 4), but the peaks are broadened significantly and the relative intensities of several major peaks are noticeably different from those of the synthetic akaganeite (Figure 1). The relative intensity of the 211 peak at 0.254 nm increased significantly compared to the other peaks in the diffraction pattern of the naturally occurring akaganeite. The broad peaks indicate much poorer crystallinity compared to its synthetic analogue. The SEM image of akaganeite shows spherical particles that are cemented together to form large aggregates (Figure 5a), which is distinctly different from the typical somatoid morphology of the synthetic akaganeite. This spherical morphology is very similar to the typical spherical pin-cushion morphology of natural schwertmannite particles.

In addition to akaganeite, goethite is another major mineral phase identified. The μ-XRD patterns of goethite show a range of crystallinities. The peak positions and intensities of well crystallized goethite match perfectly with PDF pattern 00-029-0713 (Figure 4), indicating a pure goethite phase with little or no foreign substitution. Some mismatches were observed, however, in the peak intensities in the poorly crystallized goethite diffraction pattern (Figure 4), particularly at the position around 0.255 nm (16.30º2θ) where akaganeite has its strongest 211 peak. The typical needle-shape goethite morphology was not observed in the SEM image of the soil goethite (Figure 5b). Instead, goethite was present as rough, spherical particles ~0.5 μm across, very similar to the morphology of akaganeite in the soil (Figure 5a).

Schwertmannite and jarosite were also occasionally identified (Figure 6); they were particularly abundant in the soil samples obtained during dry periods, consistent with the pH-mineral relationship discussed in the introduction. During dry periods, the redox potential increases in the soil which results in the oxidation of sulfides in the subsurface horizons. The oxidation process releases protons to the soil solution and forms acidic conditions (equation 1). The hydrolysis of Fe^{3+} further decreases the solution pH. Thus, the low-pH conditions generated through the oxidation of sulfides and the hydrolysis of Fe(III) favor the precipitation of schwertmannite and jarosite during dry periods. The identification of jarosite (Figure 6) indicates that this site once reached very acidic conditions at some stage of the seasonal redox change cycle because jarosite forms at pH < 2.5 (Bigham *et al.*, 1996). The surface morphology of jarosite is distinctly different from other secondary Fe(III) minerals identified (Figure 5c). The bipyramidal crystals are similar in size and morphology to the jarosite crystals described by Jones and Renaut (2007) in Fe-rich precipitates from acid hot springs.

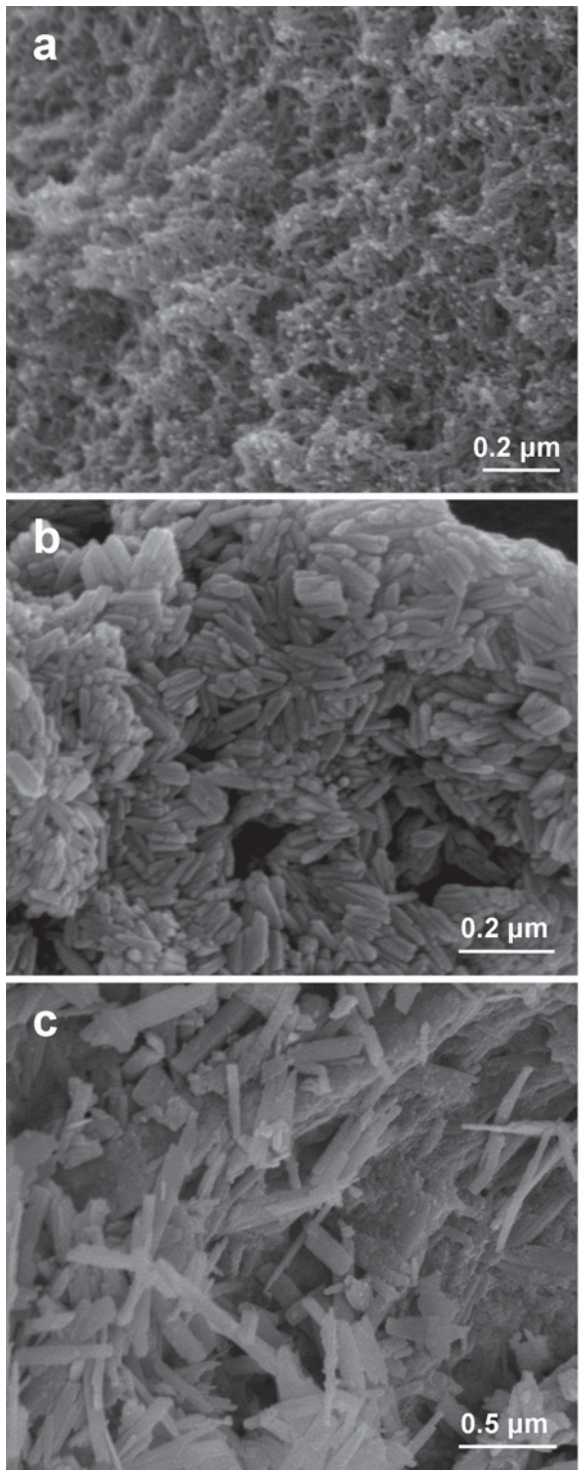

Figure 2. SEM images of synthetic (a) schwertmannite, (b) akaganeite, and (c) goethite.

The peak positions, intensities, and widths of the schwertmannite µ-XRD peaks are in good agreement with the theoretical diffraction pattern (PDF: 00-047-1775) for schwertmannite (Figure 6). Trace amounts of goethite were also present as indicated by a weak peak at d = 0.418 nm. The SEM image of soil schwertmannite shows the typical pin-cushion morphology, almost perfectly spherical, hedge-hog-like crystal aggregates ~2 µm across (Figure 5d). The small spherical particles seem to be cemented together, forming larger aggregates. Schwertmannite precipitation in soils seems to be linked directly to the bacterially catalyzed oxidation of Fe^{2+} (Kawano and Tomita, 2001). However, no bacterial cells were observed in the SEM images. The lack of observable microbial cells does not necessarily indicate an absence of microbial influence. The cells may be encased in schwertmannite particles (Schroth and Parnell, 2005). Mixtures of schwertmannite and jarosite were also identified in this soil, indicating that low-pH conditions favor the precipitation of these two minerals.

Precipitation of akaganeite

Although akaganeite has often been observed as a corrosion product of metallic iron in chloride-containing marine environments, akaganeite is rare in soils. The authors are aware of only one prior study that briefly reported the precipitation of akaganeite in an acid sulfate soil in Australia (Fitzpatrick *et al.*, 2008). However, the authors did not provide any morphological or mineralogical data for the mineral, and the mechanisms resulting in the precipitation of akaganeite were not discussed. The proposal here is that several reasons have led to the precipitation of akaganeite as one of the major secondary Fe(III) minerals at this site.

The unique pH conditions of this soil may play a key role in the precipitation of akaganeite. The soil pH is considered to be the most important factor in determining

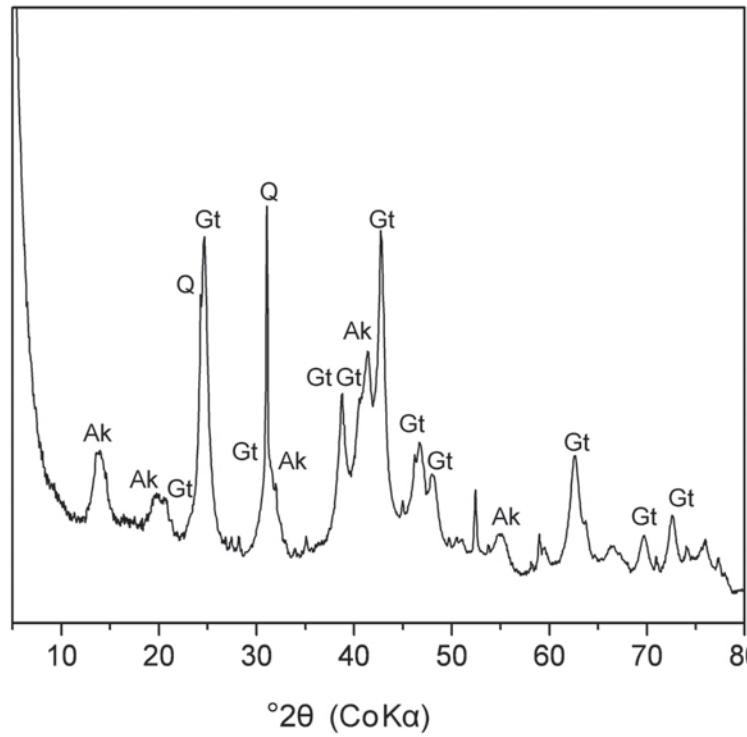

Figure 3. Bulk powder XRD pattern of the soil samples collected during a wet period. Major peaks are labeled with mineral names. Ak = akaganeite, Gt = goethite, and Q = quartz.

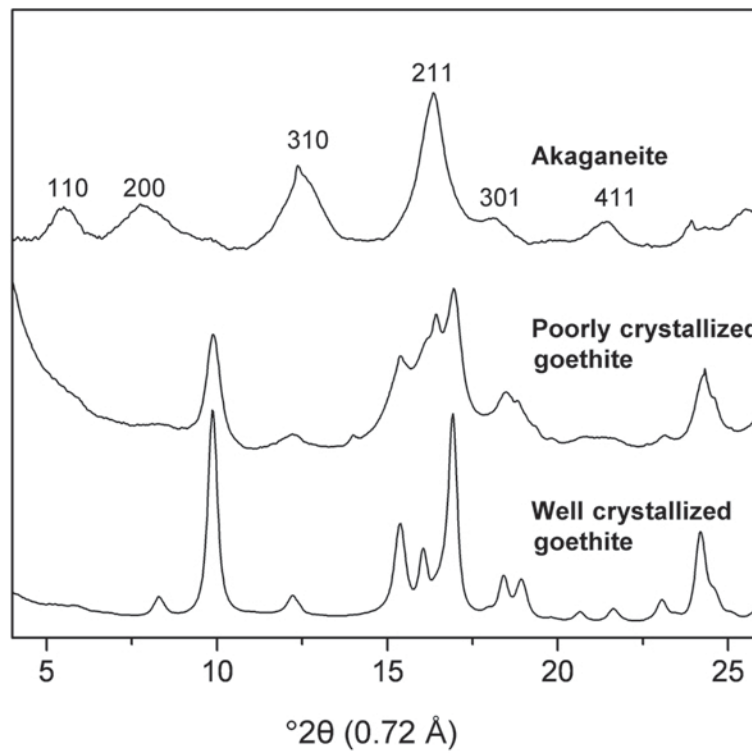

Figure 4. Synchrotron μ-XRD patterns of soil aggregates from the surface precipitates. The numbers indicate Miller indices of selected peaks.

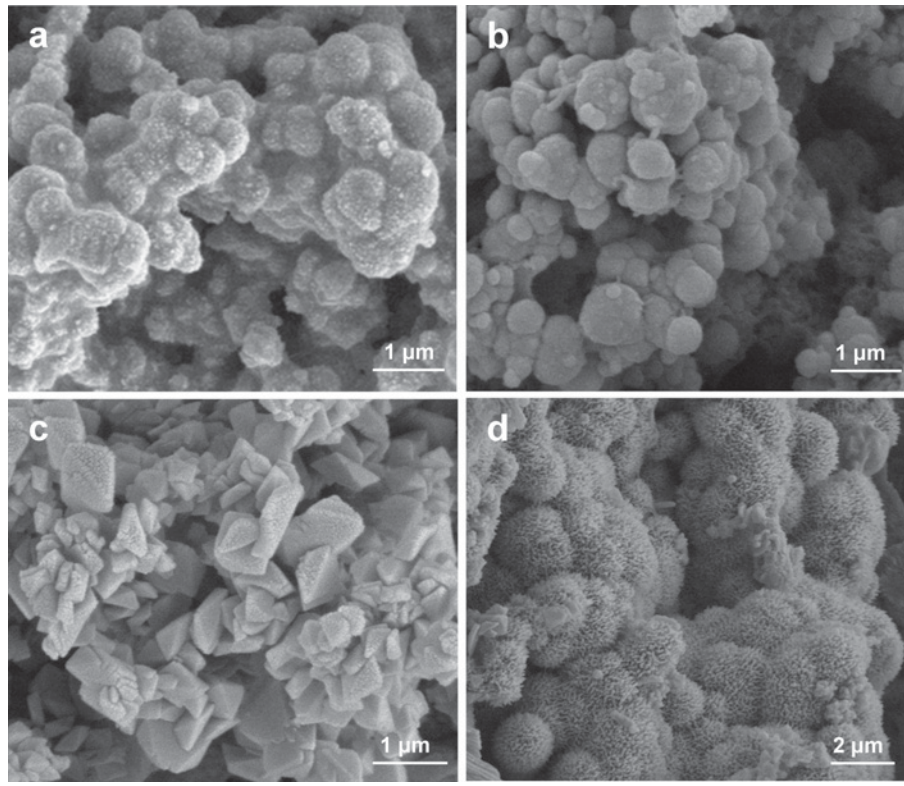

Figure 5. SEM images of naturally occurring (a) akaganeite, (b) goethite, (c) jarosite, and (d) schwertmannite, corresponding to the µ-XRD patterns of the same soil aggregates with akaganeite, well crystallized goethite, jarosite, and schwertmannite as the major phases in Figures 4 and 6.

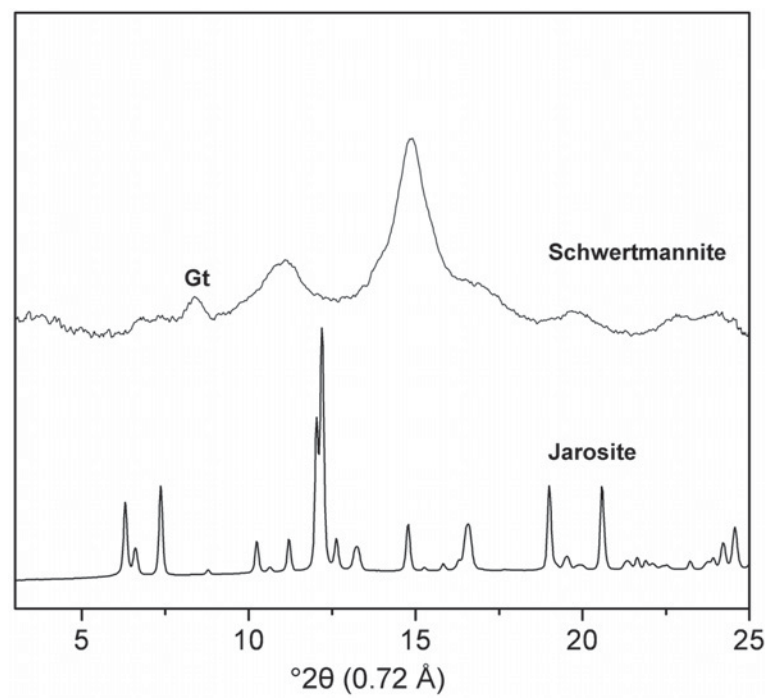

Figure 6. Synchrotron µ-XRD patterns of soil aggregates from the surface precipitates with schwertmannite and jarosite as major mineral phases. Gt = goethite.

which Fe(III) minerals precipitate (Bigham *et al.*, 1990; Bigham *et al.*, 1996; Yu *et al.*, 1999; Carlson *et al.*, 2002). The pH value of ~5.30 of the surface soil at this site is greater than the most favorable pH conditions for the precipitation of schwertmannite (pH 3−4), but is slightly less than the pH conditions for the formation of ferrihydrite (near-neutral pH) (Jonsson *et al.*, 2005). The pH of this soil, therefore, favors neither the precipitation of schwertmannite nor ferrihydrite from solution. Akaganeite, on the other hand, has been synthesized successfully in the laboratory at pH ranges from 1.5 to 8.0 (Cai *et al.*, 2001; Bakoyannakis *et al.*, 2003; Deliyanni, *et al.*, 2003), and the stability of akaganeite over this pH range makes its precipitation and persistence under the pH conditions of this soil possible.

In addition, the presence of chloride in solution is essential for the formation of akaganeite. Well crystallized, synthetic akaganeite usually contains 3−9% w/w chloride (Murad, 1979), but the crystal structure of akaganeite is not sensitive to the chloride content (Ishikawa and Inouye, 1975). Bigham *et al.* (1990) demonstrated that even when the chloride content was reduced to as low as 0.6%, the diffraction pattern still had most of the major peaks of akaganeite. The reason for this is that F^-, OH^-, and other anions can incorporate into the tunnels and stabilize the crystal structure when Cl^- is removed. Therefore, although the presence of chloride is crucial for the precipitation of akaganeite, the concentration required is much smaller than the large concentration of sulfate required to form schwertmannite. The concentrations of major anions extracted by 1:1 solid:solution aqueous extraction are shown in Table 1. The Cl^- concentration is the second largest after SO_4^{2-} and both are present at elevated levels, supporting the hypothesis that the presence of Cl^- contributes to the precipitation of akaganeite in this soil. The greater SO_4^{2-} concentration in samples collected during dry periods reflects the abundance of gypsum in these samples, which dissolves and releases SO_4^- during the extraction.

Organic matter may also play a role in this process. Nesterova *et al.* (2003) reported that a polysaccharide, alginic acid (Alg), facilitated the formation of nanocrystalline akaganeite in a model system. The soil studied is an organic-rich, wetland soil containing a variety of organic acids in the soil solution. Thus, in addition to Cl^-, organic matter may also contribute to the precipitation of akaganeite at the site in question.

Several factors resulted in the broad peaks and relative intensity changes in the akaganeite diffraction pattern. The akaganeite crystal structure is sensitive to the pH of the initial synthesis solution. Low pH favors the nucleation and growth of akaganeite crystals, while increasing pH results in the broad peaks and poor crystallinity (Cai *et al.*, 2001). Incorporation of SO_4^{2-} may also partially destroy the crystallinity of the structure, and leads to broad diffraction peaks due to the size restrictions of the structure (Bigham *et al.*, 1990; Deliyanni *et al.*, 2003). The SO_4^{2-} ion (radius = 0.23 nm) is larger than the Cl^- ion (radius = 0.18 nm). Incorporation of sulfate into the tunnels of akaganeite will distort the akaganeite structure, reduce the symmetry, reduce crystal growth, and partly change the unit-cell parameters (Jonsson *et al.*, 2005). Bigham *et al.* (1990) reported that the addition of sulfate to the initial hydrolysis solution during akaganeite synthesis broadened all peaks and reduced the intensities of the 110 and 310 peaks. At extremely high concentrations of sulfate (11.6%), the 110 peak was completely suppressed. Other oxyanions larger in size than Cl^-, *e.g.* AsO_4^{3-} (radius = 0.248 nm) and CrO_4^{2-} (radius = 0.24 nm), which are present at high concentrations in this soil (Gao and Schulze, 2010), should have similar distortion effects as SO_4^{2-} and would further destroy the crystallinity of akaganeite. With SO_4^{2-} incorporation, the 211 peak at 0.254 nm (Figure 4) became the strongest peak in the diffraction pattern, whereas the 212 peak of schwertmannite at the same position (Figure 1) is also the strongest peak in its XRD pattern.

In addition to crystal structure, large quantities of SO_4^{2-} incorporated into the structure of akaganeite also appear to have had significant impacts on its morphology. The particle morphology of akaganeite, for example, changed from somatoidal to spherical, similar to the schwertmannite morphology. The naturally occurring akaganeite described here, therefore, is like an intermediate phase between akaganeite and schwertmannite.

Transformation of the secondary Fe(III) oxyhydroxides

The poorly crystalline phases akaganeite and schwertmannite are metastable with respect to goethite and will transform to goethite with time. Although goethite could coprecipitate with other poorly crystalline Fe minerals when the sulfate concentration is small, with

Table 1. Major anion concentrations (mmol kg^{-1}) of the surface precipitates extracted by 1:1 solid/solution ratio aqueous extraction.

Samples	F^-	Cl^-	SO_4^{2-}	NO_3^-	$H_2PO_4^-$
			mmol kg^{-1}		
Wet period	5.72 ± 0.10	31.69 ± 1.78	133.91 ± 21.36	0.64 ± 0.03	0.83 ± 0.04
Dry period	4.70 ± 0.25	60.36 ± 3.52	464.52 ± 32.34	1.31 ± 0.03	0.74 ± 0.02

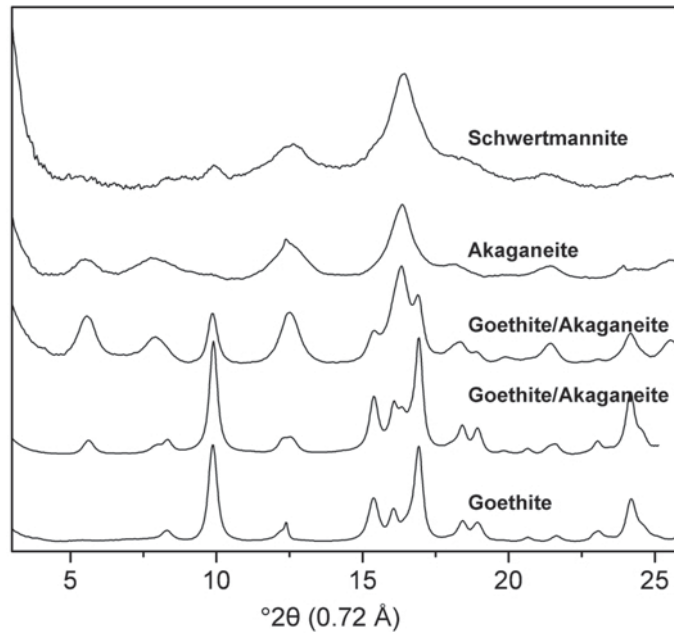

Figure 7. Synchrotron μ-XRD patterns of soil aggregates from the surface precipitates with schwertmannite, akaganeite, and goethite as the major mineral phases.

the large amount of sulfate at this site, the coprecipitation of goethite and akaganeite should be very rare (Bradley *et al.*, 1996). The goethite in the precipitates may not be the product of direct precipitation from the solution, therefore, but the transformation product of previously precipitated akaganeite or schwertmannite. The occurrence of mixtures of goethite and akaganeite is clear evidence for the transformation. The μ-XRD patterns (Figure 7) suggest the transformation processes. Fe(III) first precipitated as sulfate-incorporated akaganeite or schwertmannite, depending on soil pH and anion concentrations. It then transformed to poorly crystallized goethite. The crystallinity of the poorly crystallized goethite improved with time and finally transformed to well crystallized goethite. The occurrence of mixtures of two phases indicates that the transformation is probably still in transition and has not yet achieved a steady state.

The SEM images provide more direct evidence of the transformation from akaganeite to goethite. The goethite has a rough, spherical particle morphology (Figure 5b), which is very similar to the morphology of akaganeite. Such goethite pseudomorphs have been observed previously in acidic sulfate soils (Sullivan and Bush, 2004; Burton *et al.*, 2006) and strongly support the hypothesis that goethite is the transformed product from precursor akaganeite.

The transformation from poorly crystalline akaganeite to more ordered crystalline goethite is generally believed to result in a reduction in surface area and release of adsorbed trace metals to solution. From the μ-SXRF spectra of goethite and akaganeite (Figure 8), both types of minerals contained significant amounts of As and Pb. No apparent differences were observed in the two spectra, indicating that trace metals are somehow retained in the solid phase when akaganeite transformed to goethite and this may be explained by solid-state transformation mechanisms. The SEM images of goethite and akaganeite have very similar spherical particle morphologies with the same size, indicating that the transformation process was *in situ* and the original morphology of akaganeite and the associated metals were almost completely preserved.

CONCLUSIONS

Goethite and akaganeite were identified as the major mineral components of the precipitates in the surface horizon of an organic soil at the site of a former lead smelter. Schwertmannite and jarosite were often identified in the soil samples from dry periods. The precipitation and characterization of akaganeite in natural soils is discussed here for the first time. The study demonstrated that under favorable pH conditions and with the presence of chloride, akaganeite can precipitate in soils as a major mineral phase.

The SEM images and μ-XRD data support the hypothesis that goethite in the precipitates is the transformation product of previously precipitated akaganeite or schwertmannite. In addition, trace metals adsorbed or coprecipitated with akaganeite appear to be retained in goethite during the transformation processes, possibly due to site-specific transformation mechanisms. Further laboratory-based studies on the transformation of akaganeite to goethite are needed to understand the

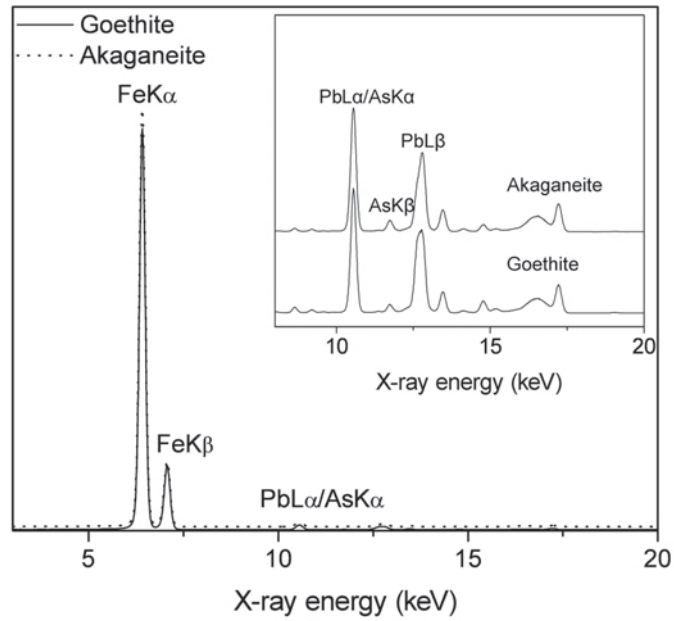

Figure 8. Synchrotron X-ray fluorescence (SXRF) spectra of soil aggregates from the surface precipitates with goethite and akaganeite as the major mineral phases. The inset figure shows the small spectral region of As and Pb fluorescence peaks.

transformation mechanisms and their impacts on the mobility and bioavailability of metals associated with them.

Within a broader context, results from this research provide some insight into understanding the long-term stability of Fe oxyhydroxides as trace-metal sinks in soils and provide very important information for the development of *in situ* chemical amendments to immobilize toxic metals with various Fe minerals.

ACKNOWLEDGMENTS

This research was funded by the U.S. Department of Defense, Strategic Environmental Research and Development Program (SERDP), Grant CU-1351. Use of the National Synchrotron Light Source (NSLS) was supported by the Department of Energy. The authors thank Tony Lanzirotti and Bill Rao for assistance with Beamline X26A at NSLS and Debra Sherman of the Life Science Microscopy Facility at Purdue University for assistance obtaining the electron micrographs. The authors thank three anonymous reviewers for helpful comments on the manuscript.

REFERENCES

Acero, P., Ayora, C., Torrento, C., and Nieto, J.M. (2006) The behavior of trace elements during schwertmannite precipitation and subsequent transformation into goethite and jarosite. *Geochimica et Cosmochimica Acta*, **70**, 4130–4139.

Bakoyannakis, D.N., Deliyanni, E.A., Zouboulis, A.I., Matis, K.A., Nalbandian, L., and Kehagias, T. (2003) Akaganeite and goethite-type nanocrystals: Synthesis and characterization. *Microporous and Mesoporous Materials*, **59**, 35–42.

Bigham, J.M., Schwertmann, U., Carlson, L., and Murad, E. (1990) A poorly crystallized oxyhydroxysulfate of iron formed by bacterial oxidation of Fe(II) in acid-mine waters. *Geochimica et Cosmochimica Acta*, **54**, 2743–2758.

Bigham, J.M., Schwertmann, U., Traina, S.J., Winland, R.L., and Wolf, M. (1996) Schwertmannite and the chemical modeling of iron in acid sulfate waters. *Geochimica et Cosmochimica Acta*, **60**, 2111–2121.

Bigham, J.M., Fitzpatrick, R.W., and Schulze, D.G. (2002) Iron oxides. Pp. 323–366 in: *Soil Mineralogy with Environmental Application* (J.B. Dixon and D.G. Schulze, editors). Soil Science Society of America, Inc. Madison, Wisconsin, USA.

Bradley, K.S., Bigham, J.M., Jaynes, W.F., and Logan, T.J. (1986) Influence of sulfate on Fe-oxide formation: Comparisons with a stream receiving acid mine drainage. *Clays and Clay Minerals*, **34**, 266–274.

Burton, E.D., Bush, R.T., and Sullivan, L.A. (2006) Sedimentary iron geochemistry in acidic waterways associated with coastal lowland acid sulfate soils. *Geochimica et Cosmochimica Acta*, **70**, 5455–5468.

Cai, J., Liu, J., Gao, Z., Navrotsky, A., and Suib, S.L. (2001) Synthesis and anion exchange of tunnel structure akaganeite. *Chemistry of Materials*, **13**, 4595–4602.

Carlson, L., Bigham, J.M., Schwertmann, U., Kyek, A., and Wagner, F. (2002) Scavenging of As from acid mine drainage by schwertmannite and ferrihydrite: A comparison with synthetic analogues. *Environmental Science & Technology*, **36**, 1712–1719.

Carroll, D. and Richmond, W.R. (2008) Incorporation of molybdate anion into β-FeOOH. *American Mineralogist*, **93**, 1641–1646.

Cornell, R.M. and Schwertmann, U. (2003) *The Iron Oxides: Structure, Properties, Reactions, Occurrence and Uses*. VCH, Weinheim, Germany.

Deliyanni, E.A. and Matis, K.A. (2005) Sorption of Cd ions onto akaganeite-type nanocrystals. *Separation and Purification Technology*, **45**, 96–102.

Deliyanni, E.A., Bakoyannakis, D.N., Zouboulis, A.I., and Matis, K.A. (2003) Sorption of As(V) ions by akaganeite-type nanocrystals. *Chemosphere*, **50**, 155–163.

Dixit, S. and Hering, J.G. (2003) Comparison of arsenic(V) and arsenic(III) sorption onto iron oxide minerals: Implications for arsenic mobility. *Environmental Science & Technology*, **37**, 4182–4189.

Fitzpatrick, R., Degens, B., Baker, A., Raven, M., Shand, P., Smith, M., Rogers, S., and George, R. (2008) Avon Basin, WA Wheatbelt: Acid sulfate soils and salt efflorescences in open drains and receiving environments. Pp 189–204 in: *Inland Acid Sulfate Soil Systems Across Australia* (R. Fitzpatrick and P. Shand, editors). CRC LEME Open File Report No. 249. (Thematic Volume) CRC LEME, Perth, Australia.

Ford, R.G. (2002) Rates of hydrous ferric oxide crystallization and the influence on coprecipitated arsenate. *Environmental Science & Technology*, **36**, 2459–2463.

Fukushi, K., Sato, T., and Yanase, N. (2003) Solid-solution reactions in As(V) sorption by schwertmannite. *Environmental Science & Technology*, **37**, 3581–3586.

Gao, X. and Schulze, D.G. (2010) Chemical and mineralogical characterization of arsenic, lead, chromium, and cadmium in a metal-contaminated Histosol. *Geoderma*, **156**, 278–286.

Ishikawa, T. and Inouye, K. (1975) Role of chlorine in β-FeOOH on its thermal change and reactivity to sulfur dioxide. *Bulletin of the Chemical Society of Japan*, **48**, 1580–1584.

Jones, B. and Renaut, R.W. (2007) Selective mineralization of microbes in Fe-rich precipitates (jarosite, hydrous ferric oxides) from acid hot springs in the Waiotapu geothermal area, North Island, New Zealand. *Sedimentary Geology*, **194**, 77–98.

Jonsson, J., Persson, P., Sjoberg, S., and Lovgren, L. (2005) Schwertmannite precipitated from acid mine drainage: Phase transformation, sulphate release and surface properties. *Applied Geochemistry*, **20**, 179–191.

Jonsson, J., Jonsson, J., and Lovgren, L. (2006) Precipitation of secondary Fe(III) minerals from acid mine drainage. *Applied Geochemistry*, **21**, 437–445.

Kawano, M. and Tomita, K. (2001) Geochemical modeling of bacterially induced mineralization of schwertmannite and jarosite in sulfuric acid spring water. *American Mineralogist*, **86**, 1156–1165.

Lazaridis, N.K., Bakoyannakis, D.N., and Deliyanni, E.A. (2005) Chromium(VI) sorptive removal from aqueous solutions by nanocrystalline akaganeite. *Chemosphere*, **58**, 65–73.

Linehan, J.C., Darab, J.G., Matson, D.W., Chen, X., and Amonette, J.E. (1997) Synthesis and characterization of akaganeite-like ferric oxyhydroxides. *Materials Research Society Symposium Proceedings*, **432**, 157–161.

Murad, E. (1979) Mössbauer and X-ray data of β-FeOOH (akaganeite). *Clay Minerals*, **23**, 161–173.

Murad, E., Schwertmann, U., Bigham, J.M., and Carlson, L. (1994) The mineralogical characteristics of poorly crystalline precipitates formed by oxidation of Fe^{2+} in acid sulfate waters. Pp. 190–200 in: *Environmental Geochemistry of Sulfate Oxidation* (C.N. Alpers and D.W. Blowes, editors). American Chemical Society, Washington, D.C.

Nesterova, M., Moreau, J., and Banfield, J.F. (2003) Model biomimetic studies of templated growth and assembly of nanocrystalline FeOOH. *Geochimica et Cosmochimica Acta*, **67**, 1177–1187.

Regenspurg, S. and Peiffer, S. (2005) Arsenate and chromate incorporation in schwertmannite. *Applied Geochemistry*, **20**, 1226–1239.

Remazeilles, C. and Refait, P. (2007) On the formation of β-FeOOH (akaganeite) in chloride-containing environments. *Corrosion Science*, **49**, 844–857.

Rhoades, J.D. (2002) Salinity: Electrical Conductivity and total dissolved solids. Pp. 417–435 in: *Methods of Soil Analysis: Part 3 Chemical Methods* (D.L. Sparks, editor). Soil Science Society of America, Inc. Madison, Wisconsin, USA.

Rohwerder, T., Gehrke, T., Kinzler, K., and Sand, W. (2003) Bioleaching review part A: Progress in bioleaching: fundamentals and mechanisms of bacterial metal sulfide oxidation. *Applied Microbiology and Biotechnology*, **63**, 239–248.

Schroth, A.W. and Parnell, R.A. (2005) Trace metal retention through the schwertmannite to goethite transformation as observed in a field setting, Alta Mine, MT. *Applied Geochemistry*, **20**, 907–917.

Singh, B., Wilson, M.J., McHardy, W.J., Fraser, A.R., and Merrington, G. (1999) Mineralogy and chemistry of ochre sediments from an acid mine drainage near a disused mine in Cornwall, UK. *Clay Minerals*, **34**, 301–317.

Sullivan, L.A. and Bush, R.T. (2004) Iron precipitate accumulations associated with waterways in drained coastal acid sulfate landscapes of eastern Australia. *Marine and Freshwater Research*, **55**, 727–736.

Webster, J.G., Swedlund, P.J., and Webster, K.S. (1998) Trace metal adsorption onto an acid mine drainage iron(III) oxy hydroxy sulfate. *Environmental Science & Technology*, **32**, 1361–1368.

Yu, J.Y., Heo, B., Choi, I.K., Cho, J.P., and Chang, H.W. (1999) Apparent solubilities of schwertmannite and ferrihydrite in natural stream waters polluted by mine drainage. *Geochimica et Cosmochimica Acta*, **63**, 3407–3416.

(*Received 17 August 2009; revised 19 March 2010; Ms. 348; A.E. T. Kogure*)